Novel laminarin-binding CBMs in multimodular proteins of marine Bacteroidota feature prominently in phytoplankton blooms

Marie-Katherin Zühlke, Elizabeth Ficko-Blean, Daniel Bartosik, Nicolas Terrapon, Alexandra Jeudy, Murielle Jam, Fengqing Wang, Norma Welsch, Robert Larocque, Diane Jouanneau, et al.

Novel laminarin-binding CBMs in multimodular proteins of marine *Bacteroidota* feature prominently in phytoplankton blooms

Marie-Katherin Zühlke[1,2*], Elizabeth Ficko-Blean[3], Daniel Bartosik[1,2], Nicolas Terrapon[4], Alexandra Jeudy[3], Murielle Jam[3], Fengqing Wang[5], Norma Welsch[1,2], Robert Larocque[3], Diane Jouanneau[3], Tom Eisenack[1], François Thomas[3], Anke Trautwein-Schult[6], Hanno Teeling[5], Dörte Becher[6], Thomas Schweder[1,2], Mirjam Czjzek[3*]

[1] Pharmaceutical Biotechnology, Institute of Pharmacy, University Greifswald, Greifswald, 17487, Germany

[2] Institute of Marine Biotechnology, 17487 Greifswald, Germany

[3] Integrative Biology of Marine Models (LBI2M), Station Biologique de Roscoff (SBR), Sorbonne Université, CNRS, 29680 Roscoff, Bretagne, France

[4] Architecture et Fonction des Macromolécules Biologiques (AFMB), Aix-Marseille Université (AMU, UMR7257), CNRS, 13288 Marseille cedex 9, Marseille, France

[5] Max Planck Institute for Marine Microbiology, Celsiusstraße 1, 28359 Bremen, Germany

[6] Microbial Proteomics, Institute of Microbiology, University Greifswald, 17487 Greifswald, Germany

[*]corresponding authors

Mirjam Czjzek, e-mail: czjzek@sb-roscoff.fr

Marie-Katherin Zühlke, e-mail: marie-katherin.zuehlke@uni-greifswald.de

Key words

carbohydrate-binding modules / glycan scavenging / laminarin / multimodular proteins / surface glycan-binding proteins

Abstract

The ß-(1,3)-glucan laminarin functions as storage polysaccharide in marine stramenophiles such as diatoms. Laminarin is abundant, water-soluble and structured simply, making it an attractive substrate for marine bacteria. As a consequence, many marine bacteria have developed competitive strategies to scavenge and decompose laminarin, which involves carbohydrate-binding modules (CBMs) as key players. We therefore functionally and structurally characterized two yet unassigned domains as laminarin-binding CBMs in multimodular proteins from our model bacterium *Christiangramia forsetii* KT0803^{T}, hereby unveiling the novel laminarin-binding CBM families CBMxx and CBMyy (official CAZy numbering will be provided upon acceptance of the manuscript in a peer-reviewed journal). We discovered four CBMxx repeats in a surface glycan-binding protein (SGBP) and a single CBMyy combined with a glycoside hydrolase module from family 16 (GH16_3). Our analyses revealed that both modular proteins have an elongated shape, and that the GH16_3 displayed a higher flexibility than the SGBP. While motility of both polypeptide chains may facilitate recognition and/or degradation of laminarin, constraints in the SGBP may support docking of laminarin onto the bacterial surface. The exploration of bacterial metagenome-assembled genomes (MAGs) from phytoplankton blooms in the North Sea revealed that both laminarin-binding CBM families are widely distributed among marine *Bacteroidota*, illustrating the high adaptability of modularity in sugar-binding and -degrading proteins. High expression of CBMxx- and CBMyy-containing proteins during phytoplankton blooms further underpins their importance in marine laminarin usage.

Introduction

Laminarin is an important energy and carbon storage compound in marine stramenophiles, including abundant diatoms. Therefore, huge amounts of laminarin are produced during common diatom-dominated phytoplankton blooms (1). Laminarin is composed of a ß-(1,3)-linked glucose backbone with occasional ß-(1,6)-linked glucose branches that differ in length and frequency (2, 3). Due to its abundance, water solubility and simple structure, marine

bacteria often prefer laminarin as a substrate over less soluble and more complex polysaccharides (4, 5). Polysaccharide utilization loci (PULs) dedicated to laminarin breakdown are thus both widely distributed (6, 7) and are highly expressed (4, 8-10) in marine bacteria that thrive during phytoplankton blooms. PULs are distinct genetic loci that encode proteins to sense, digest and transport sugars. *Bacteroidota* are key players in marine laminarin turnover and many glycoside hydrolases (GHs) active on laminarin from members of this phylum have been characterized, such as GH16 and GH17 family representatives that act on the ß-(1,3)-main chain, or GH30 family representatives that remove ß-(1,6)-side chains (11-14). Some of these GHs are bound to the cell surface, where they degrade laminarin into smaller-sized oligosaccharides suitable for uptake and transport (11). In *Bacteroidota*, the oligosaccharide shuttle to the periplasm is mediated by an accessory sugar-binding SusD-like protein, tethered to the outer membrane, and a SusC-like TonB-dependent transporter (TBDT) (reviewed in 15, 16). In complex with their target substrate, SusD-like proteins act as a hinge to relay their cargo into the SusC-like TBDT (17). In addition to SusD-like proteins, bacteria may have additional surface glycan-binding proteins (SGBPs), which are often encoded directly downstream of the *susCD*-like gene tandem and are sometimes termed 'SusE-positioned' proteins. The designations '-like' *versus* '-positioned' intend to distinguish between homologous *versus* analogous proteins, and refer to the starch utilization system (Sus) (18, 19), which marked the beginning of the era of PUL exploration. While SusD-like proteins have a single binding site and are almost entirely α-helical, SusE-positioned SGBPs may have several carbohydrate-binding modules (CBMs), which often display a ß-sandwich fold structure and function as carbohydrate docking sites. Since SusD-like proteins also classify as SGBPs, they have sometimes been named 'SGBP-A' in the literature, whereas CBM-containing SGBPs are named 'SGBP-B' (20). Some examples of mixed-linkage ß-glucan and laminarin-related SusD-like proteins and CBM-containing SGBPs have recently been thoroughly analyzed in gut strains from the *Bacteroides* genus (21). By comparison, there is only one structure for a marine laminarin-binding SusD-like protein, which recognizes ß-(1,6)-branches in laminarin (22), and marine examples of CBM-containing SGBPs that bind laminarin are lacking. As

aforementioned, unlike SusD-like proteins, CBM-containing SGBPs rarely show detectable similarity/homology (20, 21) and are thus difficult to predict. Therefore, CBM-containing SGBPs are largely overlooked and probably underestimated. In addition to SusD-like proteins and CBM-containing SGBPs, laminarin-binding CBMs are often linked to enzymes within multidomain structures (23, 24), which further underlines the importance of CBMs in marine laminarin degradation.

The laminarin-consuming *Christiangramia forsetii* KT0803^{T} (formerly *Gramella forsetii* (25)), a member of the *Bacteroidota*, has been isolated during a phytoplankton bloom in the North Sea (26). A GH16_3 and a 'conserved hypothetical protein', encoded in the *C. forsetii* laminarin PUL, were among the most abundantly produced proteins when growing on laminarin as a sole carbon source (27). Based on subproteome analyses it was suggested that the two proteins are tethered to the outer membrane and it was speculated that the 'conserved hypothetical protein', which is SusE-positioned, might function as an SGBP (27).

This study aimed to illuminate the relevance of laminarin-binding CBMs in the scavenging and processing of laminarin, which is abundantly produced during phytoplankton blooms. We therefore structurally and functionally characterized an SGBP and a GH16_3 from the marine model bacterium *C. forsetii*, both of which display novel laminarin-binding CBMs in their multimodular structure. This gave insights into specific adaptations of a non-catalytic and a catalytic protein, respectively, with respect to their roles in first steps of laminarin utilization. It further allowed us to illustrate the distribution of these CBMs in marine bacteria and their expression as a response to algae proliferation.

Results

Multidomain proteins Cf-SGBP and Cf-GH16_3

We investigated two proteins that are encoded in a laminarin PUL and that were highly produced in laminarin-grown cells of *C. forsetii* (27): a putative CBM-containing SGBP (Cf-SGBP, locus tag GFO_RS17395) and a protein containing a GH16_3 catalytic module (Cf-GH16_3, locus tag GFO_RS16360) (Fig. 1a, further information on domain nomenclature is provided in the Materials and Methods or Fig. 1b). Subproteome analyses (27) and the presence of a lipoprotein signal peptide support that both proteins are tethered to the outer membrane. Structural prediction using Alphafold2 (AF) (28) and Phyre2 (29) uncovered that the Cf-SGBP displays two Ig-like folded (ß-sandwich) modules at its N-terminus followed by four putative CBMs (I-IV) (Fig. 1b) with high sequence-similarity (47-84%), suggesting internal duplication events. The Cf-GH16_3 on the other hand is predicted to feature a single N-terminal Ig-like folded module followed by a putative CBM, with no significant similarity to CBMs of the Cf-SGBP, and the C-terminal GH16_3 catalytic domain at the C-terminus.

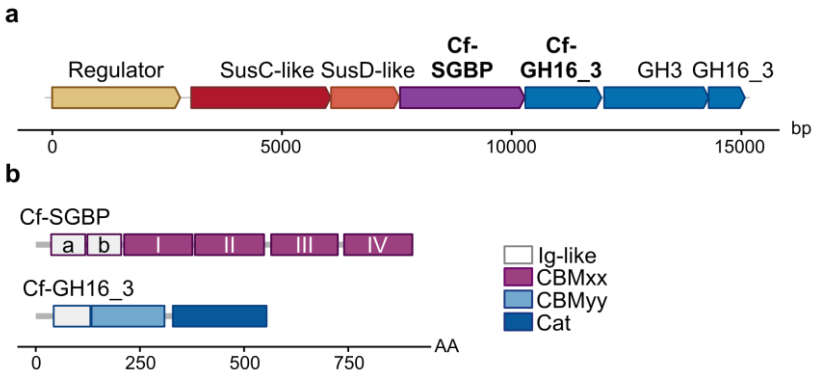

Fig. 1 The laminarin PUL of *Christiangramia forsetii* encodes the multimodular Cf-SGBP and Cf-GH16_3 containing the novel CBMxx and CBMyy, respectively. a The *C. forsetii* laminarin PUL encodes multidomain proteins, including a novel CBM-containing SGBP (Cf-SGBP) and a GH16_3 (Cf-GH16_3), highlighted bold. **b** Domain organization of the Cf-SGBP and Cf-GH16_3. Here, gray lines represent N-terminal lipoprotein signal peptides or linkers between modules. The Cf-SGBP displays two Ig-like fold modules (a,b) followed by four CBMxxs (I-IV). The Cf-GH16_3 comprises an Ig-like fold module and CBMyy in addition to its catalytic module (Cat).

All putative CBM sequences were submitted to Dali searches (30), which did not reveal any close relatives with solved 3D structures. The four CBMs from the Cf-SGBP were only remotely similar to a module attached to a GH50 from *Saccharophagus degradans* (PDB ID 4BQ2) (31), with a z-score >12 and 10-15% identity. To date, this module is not classified in any CBM

family in the CAZy classification, in the absence of a characterized close homolog. Similarly, the CBM of the Cf-GH16_3 returned uncharacterized proteins, including hypothetical CBMs, as best hits with z-scores ~8 and 9-12% sequence identity (PDB ID 4L3R and 4QRL).

Sequence analysis confirmed that the putative *C. forsetii* CBMs did not exhibit any domains belonging to a known CBM family. Hence, the functional characterization of the CBMs of the Cf-SGBP and Cf-GH16_3 (cf two following sections below) provided the basis for founding the novel CAZy (32) CBM families CBMxx and CBMyy, respectively (official CAZy numbering will be provided upon acceptance of the manuscript in a peer-reviewed journal). We determined the 3D crystal structure at 2.0 Å resolution for the isolated C-terminal CBMxx, Cf-SGBP-CBMxx$_{IV}$, in complex with laminaritriose by protein crystallography (Fig. 2a, Table S1). Least square superimposition of the corresponding AF predicted structure to the 3D crystal structure using COOT (33) and matching all atoms leads to an RMSD of 1.765. This high agreement (Fig. 2b) supported reliability for the AF predictions for the other CBMxxs, which further indicated two things: the four CBMxxs are highly similar in fold and CBMyy differs from CBMxx. The crystal structure of the Cf-SGBP-CBMxx$_{IV}$ reveals a typical CBM ß-sandwich fold, consisting of two antiparallel ß-sheets composed of four or five ß-strands that form a concave and convex face, respectively (Fig. 2a). The concave face forms a deep and narrow binding cleft, also established by two expansive loops. While the concave face contains residues mediating polar interactions with the substrate, distal loops contain aromatic residues (Fig. 2a) to establish CH-π interactions (34). AF predicted a similar fold for all four CBMxxs (Fig. 2c) and residues that mediate interaction with laminaritriose in the Cf-SGBP-CBMxx$_{IV}$ align (Fig. 2d). Remarkably, differences are seen in Cf-SGBP-CBMxx$_{III}$ loop 2, which results in a wider and very shallow binding cleft (Fig. 2c and d, Fig. S1).

Compared to the ß-sandwich-fold of CBMxx, CBMyy rather displays a ß-barrel structure with two additional α-helices and an additional β-strand pair. Together with a lacking binding groove, the *C. forsetii* CBMyy is structurally related to a CBM present in a *Bacteroidetes fluxus* SGBP (Fig. 2e, Fig. S2) (21) devoid of a catalytic GH16_3. Our analyses reveal that the *B. fluxus* CBM classifies as a CBMyy.

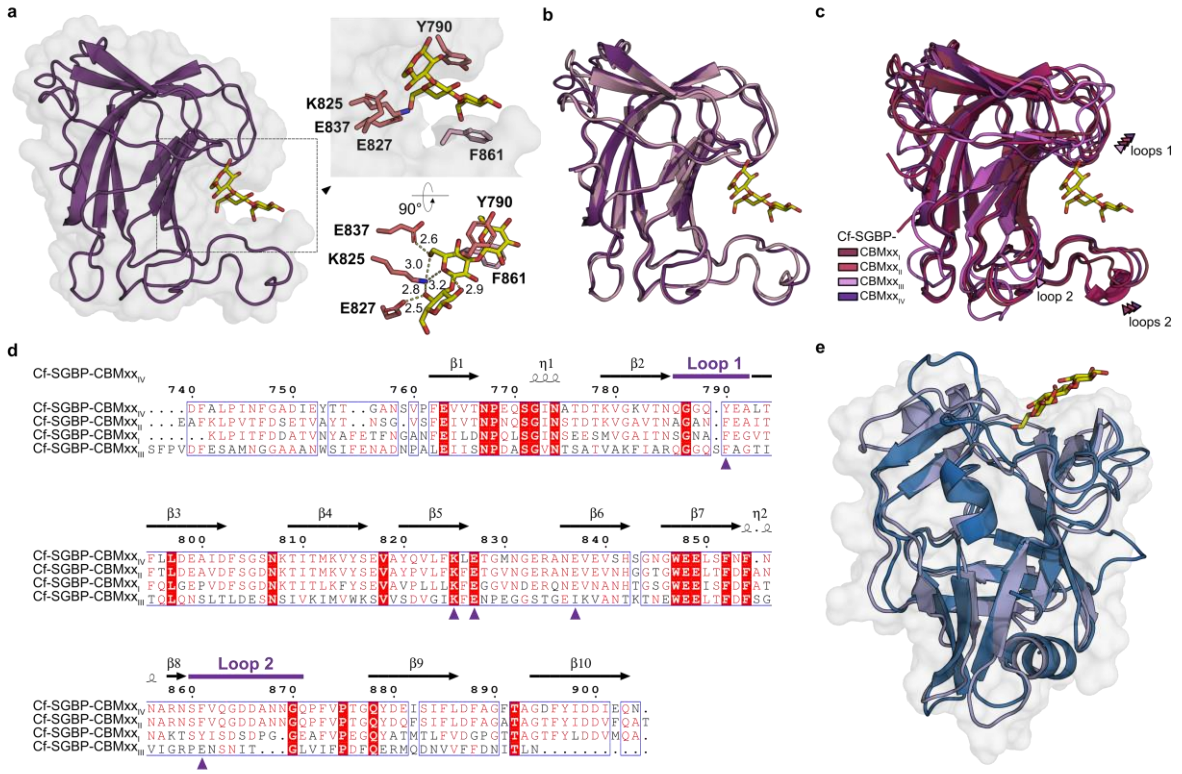

Fig. 2 CBMxx repeats of the Cf-SGBP and CBMyy of the Cf-GH16_3: binding clefts *versus* platform. a 3D crystal structure of the Cf-SGBP-CBMxx$_{IV}$ with laminaritriose, highlighting interacting residues. **b** Overlay of the crystal structure of the Cf-SGBP-CBMxx$_{IV}$ (violet) and the corresponding AF prediction (light pink), supporting the accuracy of AF. **c** Overlay of AF predicted CBMxx repeats (I-III) with the crystal structure of the Cf-SGBP-CBMxx$_{IV}$. In particular Cf-SGBP-CBMxx$_{III}$ differs in one of the loops delimiting the binding groove, which results in a flat binding region flanked only by one loop (see also Fig. S1). **d** Alignment of the Cf-SGBP-CBMxxs visualized using ESPript 3.0 (https://espript.ibcp.fr) (35). Identical residues are highlighted in red boxes, similar residues using red letters. Residues involved in substrate binding in the Cf-SGBP-CBMxx$_{IV}$ are indicated by violet arrow heads; the two loops flanking the substrate binding groove are indicated by violet lines above the alignment. **e** CBMyy of the Cf-GH16_3 displays a ß-barrel structure, missing a distinct binding cleft compared to CBMxx. The AF predicted model (blue) superimposes very closely to a CBM of an SGBP from *Bacteroidetes fluxus* (21) binding laminarin and mixed-linkage ß(1,3)/ß(1,4)-glucan on a platform (lightblue, here laminaritriose, PDB ID 7KV7, see also Fig. S2).

CBMxx and CBMyy bind laminarin

Affinity gel electrophoresis (AGE) demonstrated that the Cf-SGBP and Cf-GH16_3 bind laminarin. We narrowed down binding to the CBMs of both proteins, and excluded binding of the N-terminal Ig-like folded modules (Fig. 3a, Fig. S3 and S4). Binding to laminarin induced a distinct shift of the band for the full-length Cf-SGBP (Fig. 3b, lane 6), whereas it induced a small but distinct shift for the full-length Cf-GH16_3 with an altered, ‘mustache’-like band shape (Fig. 3b, lane 1). In comparison, the binding of the isolated catalytic domain Cf-GH16_3-Cat could not be inferred from AGE, nor was an altered band shape detected (Fig. 3b, lane 2). We hypothesize that the catalytic module releases smaller laminarin oligosaccharides that diffuse

from the gel, which is why no shift is obtained for the dissected active catalytic module. Accordingly, the shift was restored with mutants of the dissected catalytic domain (Cf-GH16_3-Cat$_{E442S}$ and Cf-GH16_3-Cat$_{E447S}$), but without the detection of the altered band shape (Fig. 3b, lanes 3 and 4). Unexpectedly, we found that the GH16_3-catalytic activity reduced the gel shift of the Cf-SGBP and resulted in a mustache-like band shape of the Cf-SGBP wherever the active enzyme was present (Fig. 3b, lanes 7 and 8). This alteration was not obtained for the Cf-SGBP loaded together with the catalytic mutants (Fig. 3b, lanes 9 and 10). We suggest that in the presence of active enzyme, the CBM-containing polypeptides (Fig. 3b, lanes 1, 7 and 8) bind to residual laminarin in-between the gel lanes, thereby modifying the shape of the bands and resulting in the ‘mustache’ effect.

In addition to laminarin binding, AGE also demonstrated binding of the mixed-linkage ß(1,3)/ß(1,4)-glucan (MLG) lichenan by Cf-GH16_3-CBMyy (Fig. S5). Activity of the Cf-GH16_3 on lichenan was not detectable by reducing sugar assay (RSA); however, fluorophore-assisted carbohydrate electrophoresis (FACE) analyses demonstrated weak activity (Fig. S6).

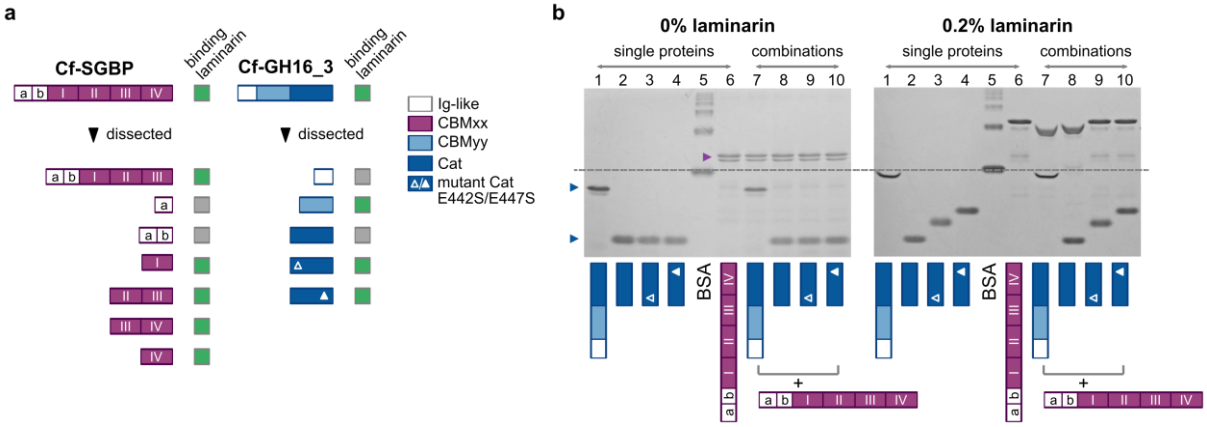

Fig. 3 Identification of laminarin-binding domains in the Cf-SGBP and Cf-GH16_3. a Summary of AGE runs, where green boxes indicate binding, which was concluded from corresponding gels in Fig. 3b, Fig. S3 and S4. **b** AGE of the Cf-GH16_3 revealed catalytic activity during runs. The Cf-GH16_3, the dissected catalytic module Cf-GH16_3-Cat and two mutants thereof (Cf-GH16_3-Cat$_{E442S}$ and Cf-GH16_3-Cat$_{E447S}$) were loaded individually (lanes 1-4) or in combination with the non-catalytic Cf-SGBP (lanes 7-10), compared to the Cf-SGBP alone (lane 6). While a shift in migration in laminarin gels indicated binding (using BSA as a control, lane 5), an altered 'mustache'-like band shape of CBM-containing proteins in laminarin gels (lane 1, 7 and 8) revealed the presence of GH16_3 activity within the lane. Detailed information is provided in the main text.

Multiple CBMxx domains in the Cf-SGBP: is 'more' really 'better'?

While the *C. forsetii* Cf-GH16_3 contains a single CBMyy to bind laminarin, the Cf-SGBP contains four consecutive CBMxxs. AGE did not provide indications on whether the higher number of CBMs in the Cf-SGBP translates into a higher binding efficiency (Fig. S3). In order to explore putative benefits of multiple CBMxx domains in more detail, we investigated laminarin binding by isothermal titration calorimetry (ITC). We selected the full-length Cf-SGBP, the tandems Cf-SGBP-CBMxx$_{II/III}$ and Cf-SGBP-CBMxx$_{III/IV}$, as well as the single module Cf-SGBP-CBMxx$_{IV}$, for which we had a 3D crystal structure, to cover a range of CBMxx repetitions for comparisons. Other constructs were either insufficiently stable or insufficiently produced and thus unfortunately not available for ITC measurements.

ITC confirmed laminarin-binding for the selected proteins (Table 1, Fig. S7a). Unexpectedly, the highest affinity for laminarin was determined for the individual Cf-SGBP-CBMxx$_{IV}$ (1.04 x 10^5 M^{-1}), which exceeded affinity of the other constructs by an order of magnitude (Table 1) and is in the same range as described for the N-terminal CBM6 of a GH16_3 (LamC) in *Zobellia galactanivorans* Dsij^T (23). A binding stoichiometry (n) of close to 0.5 indicates two CBMxx$_{IV}$s are able to interact with one ligand molecule. The binding stoichiometry is increased to ~0.75

for the double module constructs and the full-length Cf-SGBP binds 1.6 laminarin molecules per polypeptide chain, though no significantly increased affinity was seen. Instead, affinities of the full-length Cf-SGBP and the two CBMxx tandems were relatively similar (Cf-SGBP 3.09 x 10^4 M^{-1}, Cf-SGBP-CBMxx$_{II/III}$ 2.76 x 10^4 M^{-1} and Cf-SGBP-CBMxx$_{III/IV}$ 3.63 x 10^4 M^{-1}). We speculate that the increased affinity of the individual CBMxx$_{IV}$ for laminarin relative to the tandems is provided by the absence of steric/spatial inhibition of binding from the other CBMxx. Thus, in the absence of the other modules, two individual CBMxx$_{IV}$ are more optimally accommodated on the same laminarin chain. Conversely, the steric hindrance of successive CBMs in the Cf-SGBP may contribute to partial binding site inaccessibility. Furthermore, the longer constructs pay more entropic penalties than the single Cf-SGBP-CBMxx$_{IV}$, probably related to the loss of conformational freedom upon ligand binding. Notably, the Cf-SGBP-CBMxx$_{IV}$ also bound laminarin-derived oligosaccharides DP7 with a higher affinity than DP5, although with a lower affinity than laminarin (Table 1, Fig. S7b). This is coherent with increased affinity of the individual Cf-SGBP-CBMxx$_{IV}$ on laminarin, as it suggests that this CBM can accommodate more than DP7 in the ligand binding site. For all interactions, binding was enthalpy-driven, with an entropic penalty (Table 1). Confirming our results from AGE, binding of laminarin by the Cf-SGBP-Ig$_a$ was not detected.

Table 1. Affinity of laminarin (Lam) and its oligosaccharides (DP7 and DP5) to the Cf-SGBP and/or dissected modules thereof. Mean values and standard deviation (±) of ITC experiments (n≥3). Measurements were performed at 293.15 K. For each run, ΔG was calculated (Gibbs-Helmholtz equation, ΔG=ΔH-TΔS).

Cf-SGBP and selected modules - laminarin

	K_a [M^{-1}]	ΔH [kcal mol^{-1}]	ΔS [cal mol^{-1} K^{-1}]	N [sites]	ΔG [kcal mol^{-1}]
Cf-SGBP	3.09 (± 0.14) x10^4	-17.3 ± 0.11	-38.53 ± 0.46	1.60 ± 0.05	-6.02 ± 0.03
Cf-SGBP-CBMxx$_{II/III}$	2.76 (± 0.22) x10^4	-19.2 ± 1.11	-45.17 ± 3.95	0.73 ± 0.03	-5.95 ± 0.05
Cf-SGBP-CBMxx$_{III/IV}$	3.63 (± 0.44) x10^4	-18.6 ± 1.12	-42.45 ± 4.04	0.76 ± 0.04	-6.11 ± 0.06
Cf-SGBP-CBMxx$_{IV}$	1.04 (± 0.03) x10^5	-14.0 ± 0.12	-24.78 ± 0.46	0.49 ± 0.01	-6.73 ± 0.03

Cf-SGBP-CBMxx$_{IV}$ - laminarin-derived oligosaccharides (DP7 and DP5)

	K_a [M^{-1}]	ΔH [kcal mol^{-1}]	ΔS [cal mol^{-1} K^{-1}]	N [sites]	ΔG [kcal mol^{-1}]
Cf-SGBP-CBMxx$_{IV}$ DP7	1.87 (± 0.17) x10^4	-7.99 ± 0.02	-7.72 ± 0.19	0.66 ± 0.02	-5.73 ± 0.05
Cf-SGBP-CBMxx$_{IV}$ DP5	1.39 (± 0.07) x10^4	-9.14 ± 0.18	-12.20 ± 0.70	0.61 ± 0.04	-5.56 ± 0.04

Two elongated multidomain proteins allow for laminarin recognition and scavenging

The multidomain structure of the *C. forsetii* proteins and corresponding ITC experiments for the Cf-SGBP constructs raised the question about the spatial organization of their polypeptide chains. AF predictions were highly uncertain for the linkers connecting the individual modules. Therefore, we analyzed the Cf-SGBP and the Cf-GH16_3 by small-angle X-ray scattering (SAXS), which revealed that both multidomain proteins feature an elongated structural organization (Fig. 4a, Fig. S8, Table S2).

The values for the radius of gyration (R_g) and the maximum particle distance (D_{max}) derived from the scattering curve are R_g 52 Å and D_{max} 178 Å for the Cf-SGBP and R_g 38 Å and D_{max} 129.5 Å for the Cf-GH16_3 (Table S2, Fig. S8). The elongated structures were confirmed by the GASBORi (36) *ab initio* calculated envelopes (Fig. 4a, Fig. S9). All calculations for the Cf-GH16_3 returned a bent shape, while much more variable shapes were calculated for the Cf-SGBP (Fig. S9). However, the relatively high χ^2 values (all >3) of calculated individual shapes for both proteins potentially indicated that the experimental curves were not well fitted by a single envelope, which implicated possible conformational variability. Nevertheless, and using DADIMODO, spatial arrangements of the successive domains based on those predicted by AF could be determined for both the Cf-SGBP and Cf-GH16_3 that individually fitted the experimental curve (Fig. 4b and c, right panels). Superimposition of the individual models, however, covered variable arrangements (Fig. 4b and c, left panels). To further analyze the potential conformational flexibility of these proteins in solution, we used the ensemble optimization method (EOM) (38, 39). Here, an ensemble is selected from a large pool of theoretical conformers, for each of which a corresponding theoretical scattering curve is generated. The selected ensembles for both proteins were able to fit the experimental data, but in contrast to the Cf-GH16_3, the χ^2 value of the EOM fit of the Cf-SGBP (10.85 *versus* 4.57 for the Cf-GH16_3, Fig. S10) was much higher than χ^2 values of the GASBORi (Fig. 4a, Fig. S9) or DADIMODO single fits (Fig. 4b and c), indicative of lower conformational flexibility. In addition, the calculated R_{flex} for the selected ensemble of the Cf-SGBP (77%) was lower compared to that of the Cf-GH16_3 (81%), although the R_{flex} of the pool and the final R_{Sigma}

were almost the same (Table 2). R_{flex} and R_{Sigma} are values to describe the flexibility in the EOM approach, where 100% or 1 correspond to a fully flexible system, respectively. Finally, a higher flexibility of the Cf-GH16_3 was supported by shifts to higher R_g and D_{max} values for the selected ensemble compared to the pool, whereas they were biased to lower values for the Cf-SGBP (Fig. S11).

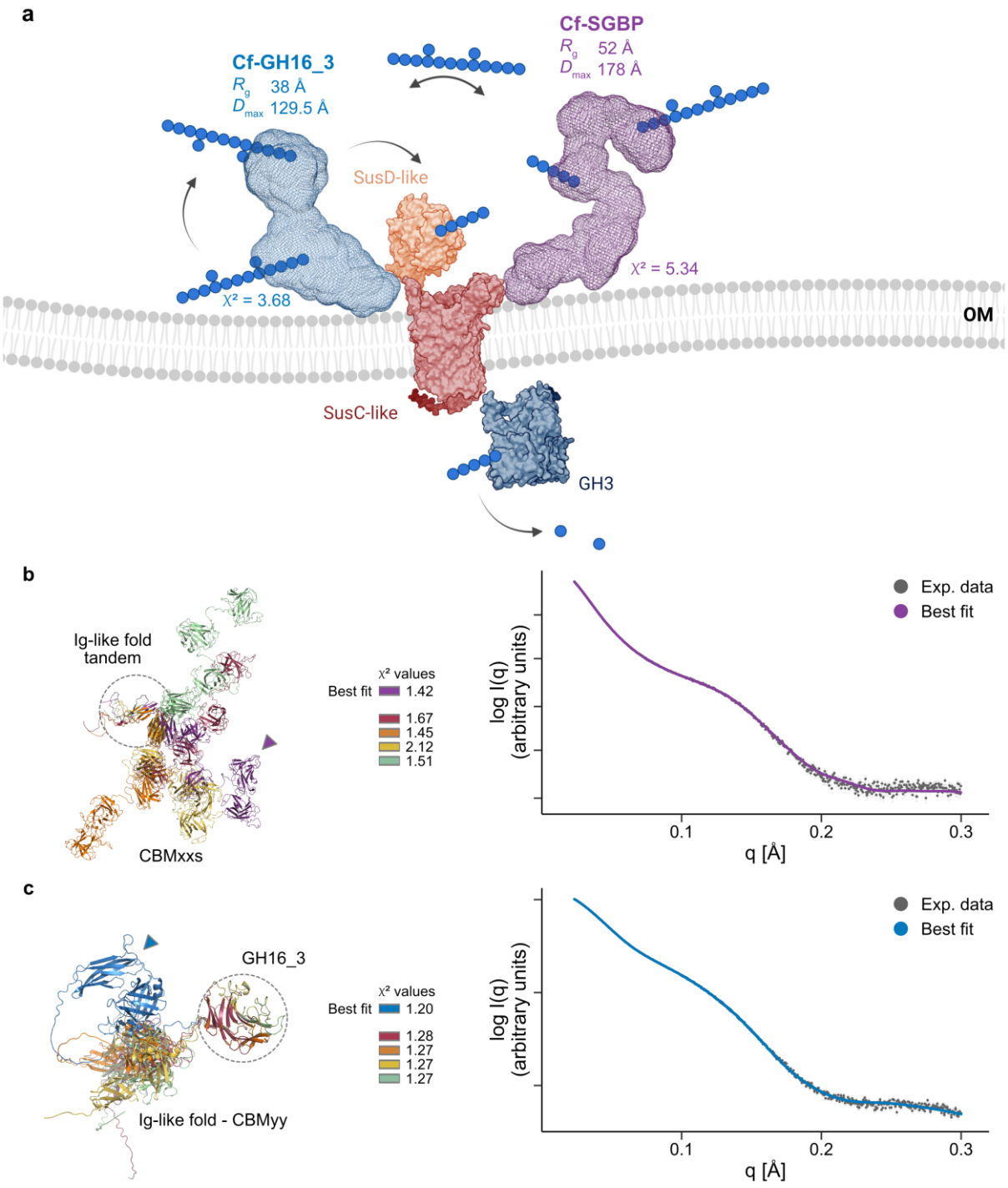

Fig. 4 Two elongated multidomain proteins to sense and capture laminarin. a R_g and D_{max} values calculated from the experimental SAXS data revealed an elongated structure for the Cf-SGBP and the Cf-GH16_3, which is also reflected in two calculated models for protein envelopes using GASBORi. The figure was created with BioRender using an adapted tentative model of laminarin utilization from (27). The spatial organization of domains in the **b** Cf-SGBP and the **c** Cf-GH16_3 was investigated using DADIMODO. Shown are five models (left graphs) in which domains used for superimposition are circled. The best fit (highest χ^2) is highlighted with an arrow head and was plotted against the experimental data (right panels). Further information on domains is provided in Fig. 1b.

Table 2 Summary of the EOM-analyses to determine the flexibility of the Cf-SGBP and the Cf-GH16_3 in solution. Given are the final R_g and D_{max} derived from the unique models for the selected ensembles, averaged R_g and D_{max} of the selected ensembles and the pool as well as R_{flex} and R_{Sigma} to describe the flexibility. R_{flex} of 100% or R_{sigma} of 1 corresponds to a fully flexible system.

	R_g [Å] final	D_{max} [Å] final	R_g [Å] ensemble	D_{max} [Å] ensemble	R_g [Å] pool	D_{max} [Å] pool	R_{flex} ensemble/pool	R_{sigma}
Cf-SGBP	52.6	175.2	53.8	175.7	58.0	189.3	77%/ 86%	0.93
Cf-GH16_3	37.7	127.6	37.6	126.6	35.6	118.7	81%/ 85%	0.94

CBMxx and CBMyy are widely distributed in Bacteroidota that thrive during phytoplankton blooms

Screening of bacterial metagenome-assembled genomes (MAGs) obtained from North Sea phytoplankton bloom-associated microbial biomass samples at Helgoland Roads in 2016, 2018 and 2020, yielded 427 sequences coding for CBMxx- and CBMyy-containing protein sequences (555 representative MAGs of which 201 belonged to *Bacteroidota*). The proportion of CBMxx-containing proteins was higher (362) compared to CBMyy (82), whereas only some sequences contained CBMxx and CBMyy (17) (Fig. 5). We found a total of 22 domain combinations, in which CBMxx and/or CBMyy were detected in protein-coding sequences with or without known catalytic modules, e.g., linked to CBM4, CBM6, GH16_3 or rare examples of GH2, GH5_34, GH5_46, GH81 and GH162. The most frequent organizations included CBMxx- or CBMyy-only-proteins (72% for CBMxx with up to eight repeats; 52% for CBMyy, always alone) followed by CBMxx or CBMyy associated with a GH16_3 (20% for CBMxx, 26% for CBMyy). In addition, corresponding sequences were frequently co-localized with genes coding for known laminarin-active enzymes, e.g., GH16_3, GH17 or GH30 family members, but also with *susCD*-like genes. Similar pictures of domain organization and genomic context for both CBMs emerged from screening draft genomes of 53 published North Sea *Bacteroidota* (6), including *C. forsetii*, as well as of the CAZy PULDB for both CBMs (as of May 2023). A total of 92 CBMxx- and/or CBMyy-containing sequences were detected in 38 of the strains from the North Sea (Fig. S12) and >400 over ~2,000 *Bacteroidota* genomes with additional relevant partners such as GH3, GH149 and GH5_46 using CAZy, strengthening this linkage. In the bloom data set, CBMxx was predominant in *Bacteroidota*, but also occurred in *Proteobacteria* or as rare exceptions in *Actinobacteriota* and *Myxococcota*, whereas CBMyy was exclusive to

315 *Bacteroidota*. This was confirmed by CAZy, which additionally showed that CBMxx and CBMyy
316 occur also in environments other than marine. Structural deviations that we have already
317 discovered in CBMxxs of the Cf-SGBP are also reflected in sequences from bacterial MAGs
318 (Fig. S13 and S14). Nevertheless, residues mediating polar interactions with the substrate in
319 the Cf-SGBP-CBMxx$_{IV}$, and also some structural residues, were highly conserved (Fig. S14).
320 Since not all putative non-catalytic proteins may be attached to the outer membrane to function
321 as CBM-containing SGBPs, we will henceforth use the term (S)GBPs.

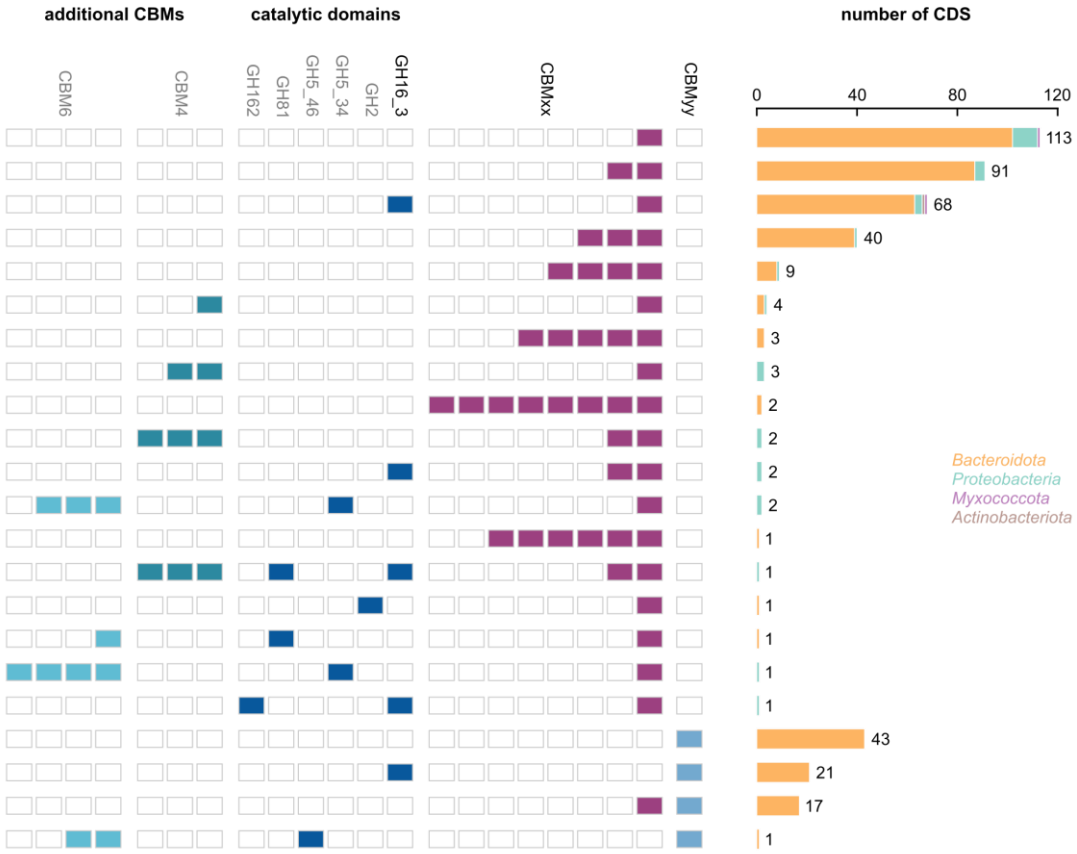

322

323 **Fig. 5. Distribution of CBMxx and CBMyy in proteins encoded in MAGs from algae blooms in the North Sea.**
324 Overview of detected CBMxx- and CBMyy-coding sequences and their co-occurrence with CBMs and catalytic
325 modules in multimodular proteins as well as the frequency of occurrence of detected domain combinations and the
326 assigned taxonomy. The graph also depicts multiplicity of certain modules, where each tile represents a detected
327 domain. Note that this graph does not represent the organization of domains within the polypeptide chain. While
328 CBMxx crossed phyla, CBMyy was restricted to *Bacteroidota* in this data set.

329

330 *Protein expression correlated with the course of the bloom*

331 Metaproteome analyses showed that the overall expression of CBMxx and CBMyy-containing
332 proteins correlated with bloom intensities (Fig. 6a and b), as assessed by chlorophyll *a*
333 measurements (40). CBM-containing (S)GBPs were more prevalent than CBM-containing
334 enzymes (mainly GH16_3s), possibly due to the higher number of putative (S)GBP sequences.
335 In addition, production of CBM-containing (S)GBPs remained more or less stable after
336 chlorophyll *a* peaks. Looking at the expression of specific laminarin PULs derived from MAGs,
337 CBMxx-containing (S)GBPs, but also CBMyy-containing GH16_3s were detected with a high
338 coverage, while other PUL-encoded GHs were often not captured (e.g., GH3, GH17 or
339 GH30_1). Moreover, CBMxx- and CBMyy-containing proteins were highly abundant in
340 metaproteomes, sometimes comparable to the expression of SusC/D-like 'marker' proteins
341 (Fig. 6c).

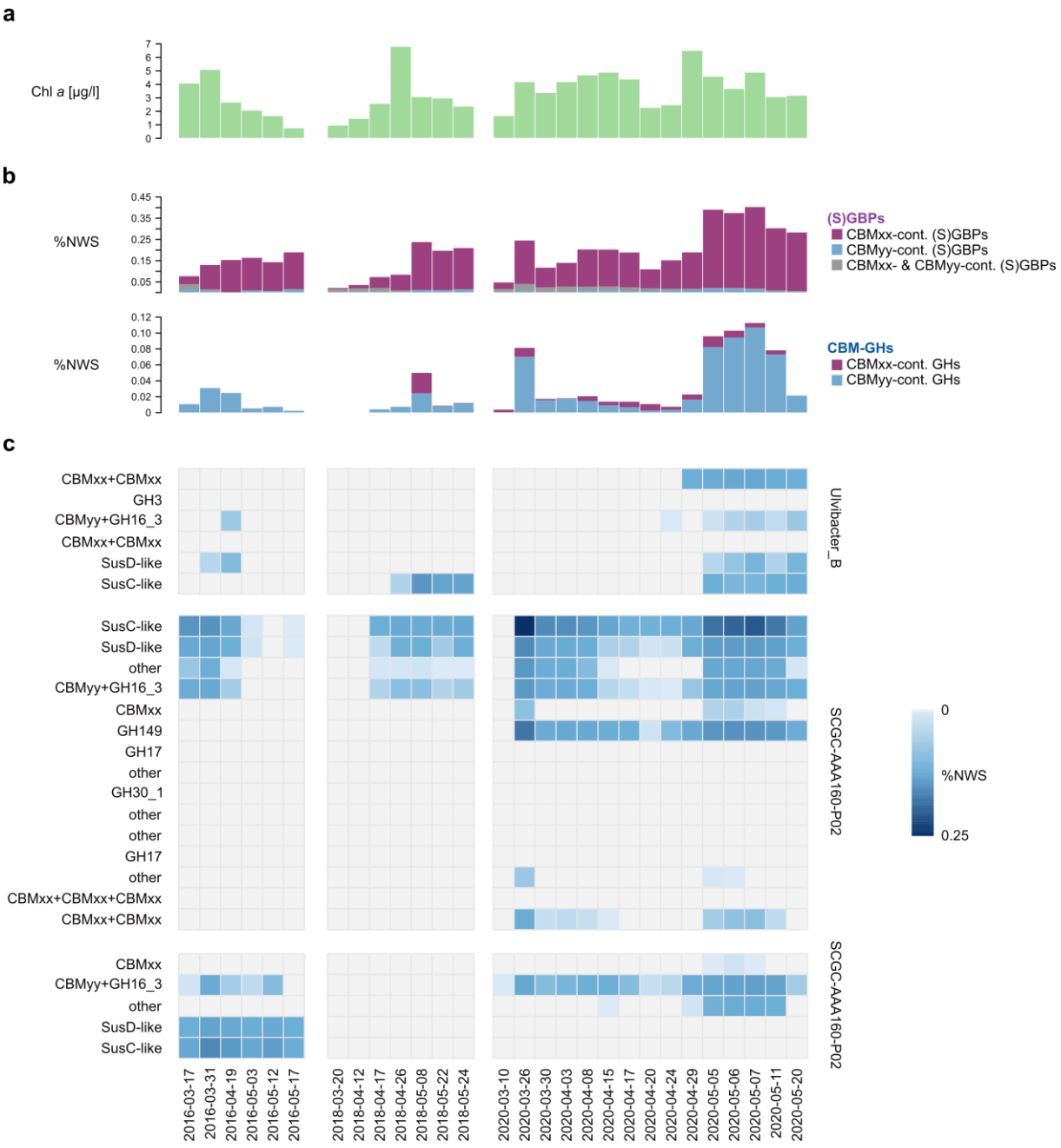

Fig. 6 Expression of CBMxx- and CBMyy-containing proteins correlates with the course of phytoplankton blooms. Data show chlorophyll *a* measurements (40) and results of semi-quantitative metaproteome analyses (0.2 µm bacterial fractions) from three respective years, see Material and Methods. **a** Course of the bloom illustrated using the chlorophyll *a* concentration. **b** Summed protein abundance values (%NWS, normalized weighted spectra) for CBMxx- or CBMyy-containing proteins. The upper graph depicts putative (S)GBPs, containing CBMs only, and the lower graph depicts CBM-containing catalytic proteins. Please note different scales (%NWS) for both graphs. **c** Abundance of proteins encoded by three selected laminarin PULs. Gray tiles correspond to proteins that were not quantified.

Discussion

Elevated photosynthetic primary production during marine phytoplankton blooms lead to pronounced increases in available substrates and nutrients to marine bacteria. These include a plethora of polysaccharides where laminarin is particularly abundant (1). The surface of many bloom-associated bacteria is therefore equipped with specific sugar-binding and -degrading proteins to ensure the recognition and docking of target substrates to the cellular surface, to allow first steps of enzymatic catalysis, but also to prevent loss of small-sized oligosaccharides that need to be shuttled into the cell. The successful and specific binding of poly- and oligosaccharides is therefore a key process in bacterial polysaccharide degradation that can only be understood by detailed analyses of the CBMs involved, as exemplified in this study by the two novel laminarin-binding families CBMxx and CBMyy.

CBMxx and CBMyy bind laminarin, but belong to different 3D folds

CBMxx and CBMyy both bind to laminarin, but differ substantially in sequence and structure. All four CBMxxs of the Cf-SGBP exhibit a ß-sandwich fold that provides a distinct binding cleft. At the same time, differences in the surrounding loops result in variation of the wideness and depth of the cleft. While $CBMxx_{I/II/IV}$ display a deep and narrow cleft, it is much shallower in $CBMxx_{III}$. This is consistent with observations in other multidomain proteins with multiple CBMs of the same family, e.g., the CBM22 tandem in a xylanase from *Paenibacillus barcinonensis* (41). Here, a wider groove in one of the CBM22 units was suspected to allow for binding of larger decorations. Screening of MAGs of bloom-associated bacteria for CBMxx sequences revealed similar structural variations that may affect either binding specificity or affinity. In contrast to the common ß-sandwich fold of the CBMxx, the ß-barrel fold of the CBMyy is rather rare in CBMs. The latter has recently been described in a CBM-containing SGBP from *B. fluxus,* which can now be classified as a CBMyy. Interestingly, in addition to laminarin, the Cf-GH16_3-CBMyy was also able to bind MLG lichenan, as previously observed for the *B. fluxus* protein (21). Moreover, the Cf-GH16_3-CBMyy lacks a distinct cleft. In the case of the *B. fluxus* protein, binding of ß-glucan termini occurred on the top of the ß-barrel, in a very shallow cleft

or platform (21), which we likewise suggest for the *C. forsetii* protein (Fig. S2). This binding site, distally positioned within the loop regions connecting the successive β-strands of the barrel core, is to some extent comparable to that of some CBM6 (42) or CBM32 (43) members, and of several lectin classes (https://unilectin.unige.ch/unilectin3D/). In summary, CBMxx classifies as a type B CBM, probably with more or less possibility to accommodate branches, while CBMyy classifies as a type C CBM (44).

Shape and flexibility of CBMxx- and CBMyy-containing proteins facilitate recognition and processing of laminarin

The laminarin-binding CBMxx and CBMyy are arranged in elongated shapes of multimodular proteins. In the case of the Cf-SGBP, with its four CBMxxs, the protein may tower out other outer membrane proteins, literally reaching out for its target substrate (Figure 4a). Elongated shapes of multimodular CBM-containing SGBPs have been determined before, e.g., for an SGBP in a heparin/heparan sulfate PUL from *B. thetaiotaomicron* (45). Like the Cf-SGBP (SAXS: R_g 52 Å and D_{max} 178 Å), the *B. thetaiotaomicron* protein consisted of six distinct domains and SAXS determined similar spatial expansions (R_g of 44.3 Å and D_{max} of 150 Å). In addition to the elongated shapes, analyses revealed a bent shape for CBMyy-containing Cf-GH16_3 (R_g 38 Å and D_{max} 129.5 Å), seen before in another multidomain laminarinase from *Thermotoga petrophila* (CBM-GH16-CBM, R_g 40 Å and D_{max} 130 Å) (46). Our results also indicated that both proteins are flexible to some extent, albeit with a higher flexibility for the Cf-GH16_3. The increased flexibility may be due to missing prolines in the Cf-GH16_3 linkers, as central prolines are suggested to hamper flexibility (45, 47). Such prolines are present in linkers between CBMxxs in the Cf-SGBP. It was speculated that this rigidity enables distance to the membrane and thus an improved exposure of the sugar-binding site (47). This might be further supported by Ig-like fold domains that could act as spacers to the outer membrane (21). Such a projection of SGBPs into the extracellular space has recently been shown for a fructan-specific SGBP from *B. thetaiotaomicron* in a complex with a GH32 and SusC/D-like proteins, called the ‘utilisome’ (48). Compared to the fructan-specific SGBP, which contains one CBM,

406 the laminarin-specific Cf-SGBP from *C. forsetii* provides four CBM docking sites. However, our
407 analyses indicated binding of two laminarin chains at maximum, possibly due to steric inhibition
408 of binding due to the other CBMs. Nevertheless, equipping the cellular surface with SGBPs
409 that contain multiple CBMs increases binding opportunities in 3D space and might optimize
410 the presence of proteins on the bacterial surface as a competitive advantage compared to
411 single CBM-containing SGBPs. Moreover, multiple binding sites in SusE and SusF are known
412 to compensate for decreased binding due to polysaccharide capsules in gut bacteria (49). This
413 may be transferable to the marine counterpart, which is also known to produce
414 exopolysaccharides (50). In the fructan utilisome the sugar chain was held by an accessory
415 tethering side of the GH32 and by the SGBP. The GH32 catalytic activity then cuts between
416 both held ends, which was suggested to facilitate degradation (48). In general, the
417 advantageous effect of CBM-enzyme co-occurrence has largely been demonstrated (e.g., 51,
418 52). CBMs may also prevent the loss of released degradation products by serving as a short-
419 term cache for cleaved sugars, which are then further digested or translocated to the SusC/D-
420 like transporters (Fig. 4a). At the same time, the affinity of laminarin-derived oligosaccharides
421 to the Cf-SGBP-CBMxx$_{IV}$ was lower, as also observed for a CBM6 from *Z. galactanivorans*
422 Dsij^{T} (23), which supports its major role in capturing laminarin.

423 *Vivid exchange and combination of domains to increase fitness*

424 Our data from phytoplankton bloom-associated bacteria show that the *C. forsetii* proteins are
425 representatives of diverse domain organizations of both CBMs in multimodular catalytic
426 proteins, mostly GH16_3s, and putative non-catalytic proteins of which a proportion might
427 function as SGBPs. This suggests a rather dynamic intermixing of CBMs by translocations,
428 duplications or losses, which causes also turnovers between catalytic and non-catalytic
429 proteins. Structural variability of CBMs further contributes to this diversity, which may
430 determine substrate specificity and/or affinity. This spectrum of domain combinations and
431 protein structures in sugar-catching and processing proteins likely increases competitiveness
432 to also encounter structurally similar substrates, such as different laminarins or other ß-

glucans. The environmental relevance of these novel laminarin-binding CBM families CBMxx and CBMyy was further reflected by a good coverage of corresponding proteins during phytoplankton blooms, which was so far mostly observed for SusC/D-like proteins and GH16_3s associated to laminarin degradation (4, 8). Protein expression of laminarin-binding CBMxx- and CBMyy-containing proteins correlated with the overall intensity of the investigated blooms, supporting their role in marine laminarin use.

In summary, marine bacteria employ CBM-containing enzymes and SGBPs on their cellular surface to scavenge laminarin from the water column. This is facilitated by elongated shapes of these multimodular proteins, where a higher flexibility of the polypeptide chain may increase catalytic activity. In comparison, multiple CBMs and the limited flexibility of SGBPs may allow the accumulation of laminarin, making SGBPs optimal sugar-trapping antenna to further enhance catalysis. Together with the wide distribution and high expression of CBMxx- and CBMyy-containing proteins during phytoplankton blooms, our findings corroborate the key role of the two novel CBMs in laminarin utilization.

Materials and Methods

Carbohydrates

Laminarin (*Laminaria digitata*) was acquired from Sigma-Aldrich (Merck kGaA, Darmstadt, Germany) and MLG lichenan (Icelandic Moss) from Megazyme International Ltd. (Bray, Ireland). Laminarin-derived oligosaccharides were produced following the protocol from Jam *et al.* (23) using a GH16_3 (LamA) from *Zobellia galactanivorans* Dsij^T (13).

Nomenclature

We refer to the full-length surface glycan-binding protein, which is SusE-positioned in the laminarin PUL of *Christiangramia forsetii* KT0803^T, as Cf-SGBP (locus tag GFO_RS17395). The PUL further encodes two GH16_3s. Subject of this study was the GH16_3 encoded downstream of the Cf-SGBP, which we refer to as Cf-GH16_3 (locus tag GFO_RS16360). The two proteins display a multidomain structure and specific domains were further specified, e.g.,

Cf-GH16_3-Cat refers to the catalytic module of the Cf-GH16_3. In the case of repetitive domains of the Cf-SGBP, these modules were enumerated either alphabetically for Ig-like fold domains or with Roman numerals for the CBMxxs, starting from the N-terminus and indicated as subscripts, e.g., Cf-SGBP-Ig_a refers to the first of two N-terminal Ig-like fold domains of the Cf-SGBP. Whenever we refer to an SGBP in the text, we refer to CBM-containing SGBPs, excluding SusD-like proteins.

Cloning and site-directed mutagenesis

We used Alphafold2 (28) and Phyre2 (29) to spatially define individual modules of the two multidomain proteins. LipoP (53) detected signal peptides and MeDor (54) predicted protein disorder by hydrophobic cluster analysis. In combination, these tools served to define suitable cloning sites to express full-length proteins, individual domains or combinations thereof. Corresponding genes were amplified from *C. forsetii* genomic DNA by PCR using primers listed in Table S3. The PCR products were cloned into expression vectors pRF3 (ampicillin resistance) or pET28a (kanamycin resistance) by restriction-ligation to produce recombinant N-terminal hexa-histidine tagged proteins. The vector pRF3 is a derivative of pFO4 (55). The full-length *Cf-SGBP* and *Cf-GH16_3* were cloned into pRF3. PCR-products were digested using BamHI and AvrII, and the pRF3 vector using BamHI and NheI. In all other cases, PCR products and the pET28a vector were digested using NdeI and SacI. Digested PCR-products were ligated into expression vectors using T4 DNA ligase. Corresponding plasmids for Cf-SGBP-$Ig_{a/b}$, Cf-SGBP-$CBMxx_I$, Cf-GH16_3-Ig and Cf-GH16_3-CBMyy in pET28a, including NdeI and SacI restriction sites, were designed and ordered from GenScript (GenScript Biotech, Netherlands).

In addition, we generated two mutants of the Cf-GH16_3-Cat, where each catalytic glutamic acid was replaced by a serine, Cf-GH16_3-Cat_{E442S} and Cf-GH16_3-Cat_{E447S}. This was achieved in two steps: first, two separate reactions of PCR, using the Cf-GH16_Cat-encoding plasmid as a template, were carried out to produce the mutant gene as two overlapping fragments (F1 and F2). The purified PCR products F1 and F2 were then used as a template

for a final PCR to produce the fused product. To produce the overlapping fragments, we used a forward primer for the first fragment (F1), which annealed to the vector backbone directly upstream of *Cf-GH16_3-Cat*, and a reverse primer for the second fragment (F2), which annealed to the vector backbone downstream of *Cf-GH16_3-Cat* (designated as vector primers, Table S3). These primers were combined with a forward (F2) or reverse (F1) primer that contained the corresponding desired mutation and that annealed to the intended region of the mutation (Table S3). The purified PCR products F1 and F2 were digested with DpnI to remove any residual parental DNA before a final PCR fused F1 and F2 using the vector primers. PCR products were digested with NdeI and SacI and cloned into pET28a as described before.

Sequence identity for all constructs and successful mutation was verified by sequencing (Eurofins Genomics, Ebersberg, Germany). Plasmids were transformed into propagation strains *Escherichia coli* DH10B or DH5α before being transformed into the expression strain *E. coli* BL21(DE3).

Protein overexpression and purification

The Cf-SGBP and the Cf-GH16_3 were produced in ZYP-5052 auto-induction medium (56), supplemented with 100 µg ml^{-1} ampicillin, for 72 h at 20 °C and 130 rpm. For the production of the other proteins, clones were cultured in LB, supplemented with 30 µg ml^{-1} kanamycin, at 37°C and 130 rpm until IPTG induction (1 mM) and then at 20 °C and 130 rpm overnight. Cells were harvested by centrifugation and pellets were stored at -20 °C until protein purification. Cells were disrupted by chemical lysis. In brief, the cell pellet was suspended in resuspension buffer (50 mM MOPS pH 8.0, 25% sucrose, lysozyme) and agitated for 15 min at 4°C. Then, double the volume of lysis buffer (20 mM MOPS pH 7.5, 100 mM NaCl, 1% sodium DCA, 1% Triton-X) was added, followed by another incubation of 5 min at 4°C. $MgCl_2$ concentration was adjusted to 5 mM and samples were incubated with DNase at room temperature until viscosity of the sample decreased. Cell debris was removed from protein extract by centrifugation. Protein extract was loaded onto Histrap HP columns (Cytiva, Vélizy-Villacoublay, France)

equilibrated in buffer A (200 mM NaCl, 10 mM MOPS pH 7.8, 20 mM imidazole) and charged with 0.1 M $NiSO_4$. In general, 1 ml columns were used for a culture volume of 250 ml and 5 ml columns for 1 l of culture. Proteins were eluted with a linear gradient of 0-100% buffer B (200 mM NaCl, 10 mM MOPS pH 7.8, 500 mM imidazole) within 30 min (1 ml column) or 60 min (5 ml column) at a flow rate of 1 ml min^{-1}. For SAXS analyses, crystallography or in case of impurities, the quality of the protein sample was further increased by size exclusion chromatography (SEC) using a Superdex 200 16/60 column (Cytiva) in buffer C (200 mM NaCl, 10 mM MOPS pH 7.8). Otherwise, samples were desalted on a Hiprep 26/10 desalting column (Cytiva) in buffer C. Buffers used to purify the proteins for SAXS analyses contained 100 mM NaCl. Samples were evaluated by SDS-PAGE. Protein concentration was determined on a Nanodrop Spectrophotometer using the molecular weight and the extinction coefficient. If necessary, samples were concentrated at 3,500 rpm and 4°C using Amicon Ultra centrifugal units (Merck).

Affinity gel electrophoresis (AGE)

Prior to AGE, concentration of NaCl was decreased from 200 mM to 20 mM by diluting the protein sample with 10 mM MOPS (pH 7.8). Recombinant proteins and BSA, which served as a non-binding control, were loaded on 12% native gels without the addition of any carbohydrate, or supplemented with 0.2% laminarin or 0.1% lichenan. Runs were performed at 80 V and 4°C on ice. Proteins were stained using Coomassie Blue. Differences in length of running fronts were considered to evaluate binding.

Enzyme activity

3,5-dinitrosalicylic acid (DNS) reducing sugar assay (57) was used to confirm activity of the Cf-GH16_3 on laminarin and MLG lichenan. Proteins (20 mM NaCl, 10 mM MOPS pH 7.8) were mixed with 0.5% laminarin or lichenan (20 mM NaCl, 10 mM MOPS pH 7.8) in 200 µl reactions. Samples were incubated overnight at room temperature and therefore experiments correspond to endpoint measurements. The non-catalytic Cf-SGBP and samples without the addition of protein served as controls. 100 µl of DNS reagent was added to 100 µl of sample. After 5 min

of incubation at 95 °C, the reaction was stopped by adding 800 µl of water. Absorbance was measured at 540 nm and increased with catalytic activity. Experiments were performed in triplicates. Absorbance did not increase in the Cf-GH16_3 incubations with MLG lichenan. In this case, samples were further investigated by fluorophore-assisted carbohydrate electrophoresis (FACE) that allows for higher sensitivity. 50 µl of the overnight incubations were dried under vacuum and mixed with 2 µl of 0.15 M 8-aminonaphtalene-1,3,6-trisulfonate (ANTS) and 2 µl of 1 M $NaBH_3CN$. Samples were incubated at 37 °C in the dark for at least 2 h and dried under vacuum. After resuspension in 20 µl of 25% glycerol, 5 µl were loaded onto 27% acrylamide gels and migrated at 200 V and 4 °C. Results were visualized under UV.

Isothermal titration calorimetry (ITC)

Proteins were dialyzed against 100 mM NaCl, 10 mM MOPS pH 7.8. The dialysis buffer was used to prepare laminarin and laminarin-derived oligosaccharide solutions, as well as for washing of the ITC cell and for controls. Prior to measurements, samples and solutions were centrifuged for degassing and removal of putative protein aggregates. In addition, protein samples were evaluated by SDS-PAGE and Nanodrop repeatedly. ITC was done on a MicroCal^{TM} ITC 200 machine. Laminarin or laminarin-derived oligosaccharides were injected into 200 µl of protein, which was loaded into the sample cell. 2.5 mM of laminarin was injected into 147.6 µM of the Cf-SGBP, into 127.7 µM of the Cf-SGBP-CBMxx$_{II/III}$ or into 94.7 µM of the Cf-SGBP-CBMxx$_{III/IV}$. 1 mM of laminarin was injected into 147.5 µM of the Cf-SGBP-CBMxx$_{IV}$. For calculations with laminarin, we used the average molecular weight of laminarin from *Laminaria digitata* (2). In addition, 5 mM of laminariheptaose (DP7), 10 mM of laminaripentaose (DP5) and up to 20 mM of laminaribiose (DP2) were injected into 359.6 µM of the Cf-SGBP-CBMxx$_{IV}$. Settings were as follows: cell temperature 20 °C (293.15 K), reference power 10 µCal/s, stirring speed 750 rpm, filter period 1 sec, injection spacing 300 sec, 1 µl injection volume (first injection 0.3 µl), 35 injections in total. Experiments were performed in at least triplicates. 2.5 mM and 5 mM of laminarin were injected into 118.8 µM of the Cf-SGBP-Ig$_a$ as a non-interacting control. Titrations of buffer into proteins, laminarin into buffer or buffer into

buffer represented additional controls. MICROCAL ORIGIN v. 7 was used to analyze the data. A single-site binding model was selected.

SEC-SAXS

SAXS data of the Cf-SGBP and the Cf-GH16_3 were collected at the Synchrotron SOLEIL on the SWING beamline. Protein samples were centrifuged prior to analyses to remove putative aggregates. SAXS measurements were coupled with prefixed SEC. The SEC column was equilibrated in buffer C (100 mM NaCl, 10 mM MOPS pH 7.8), which was used for protein purification. 70 µl of protein were injected, the Cf-SGBP at 8.2 mg ml^{-1} and the Cf-GH16_3 at 12.9 mg ml^{-1}. The sample-detector-distance was 2.4 m, resulting in a scattering vector *q*-range of 0.012 – 0.504 $Å^{-1}$ for the Cf-SGBP and 0.017 – 0.504 $Å^{-1}$ for the Cf-GH16_3. The obtained scattering data were normalized and corrected according to standard procedures. The Guinier equation was used to calculate the forward scattering *I(0)* and the radius of gyration R_g. The distance distribution function *P(r)* and the maximum particle dimension D_{max} were calculated by Fourier inversion of the scattering intensity *I(q)* using GNOM integrated in the PRIMUS software (ATSAS 3.1.3) (58). Models of protein envelopes were calculated from the experimental scattering curves using GASBORi (36). High χ^2 values indicated flexible proteins. Therefore, the data were analyzed using DADIMODO (37). Here, structural data of proteins are included into the analysis to identify an arrangement that best describes the experimental data. For this, rigid bodies and linkers were defined based on the structures predicted by Alphafold2 (28). Finally, EOM analysis was used to describe the flexibility of proteins in solution (38, 39), again using Alphafold2-derived coordinates. Experimental and processed data were visualized in R using the ggplot2 package.

Crystallography

Crystallization for both recombinant constructs of Cf-SGBP-CBMxx$_{IV}$ (at a concentration of 11.7 mg ml^{-1}) and Cf-SGBP-CBMxx$_{III/IV}$ (at a concentration of 9.5 mg ml^{-1}) were tempted, in presence or absence of laminarin oligosaccharides (DP3/4), but never led to crystals in the case of Cf-SGBP-CBMxx$_{III/IV}$. Crystallization screening was undertaken with the nanodrop-

robot Crystal Gryphon (Art Robbins instruments) starting with sparse matrix sampling kits JCSGplus, PACT, PEGs, and Wizard Classic I/II and Ligand-Friendly Screen (from Qiagen and Molecular Dimensions). The initial crystallization conditions were manually optimized and suitable crystals of Cf-SGBP-CBMxx$_{IV}$ in presence of laminarin-trisaccharides were obtained using the hanging drop vapor diffusion method as follows: 2 µl of protein were mixed with 1 µl of reservoir solution (500 µl) containing 2.5 M ammonium sulfate, 0.1 M BIS-TRIS propane pH 7.0, 6% ethanol and 4% polyethylenglycol (PEG) 6000. Diffraction data were collected on PROXIMA1 (SOLEIL synchrotron) with a single crystal of Cf-SGBP-CBMxx$_{IV}$ in complex with laminarin-trisaccharide at 1.9 Å resolution. The data were integrated using XDS (59) and scaled with aimless (60). The structure was solved by molecular replacement with Phaser (61) using the AF model as starting point. The crystal structure was further enhanced with alternating cycles of refinement with REFMAC (62) and manual construction using COOT (33). All further data collection conditions and refinement statistics are given in Table S1.

Phytoplankton bloom data

Chlorophyll *a* concentration as well as metagenomes, metagenome-assembled genomes and metaproteomes were obtained from samples taken during spring phytoplankton blooms at North Sea island of Helgoland in 2016 (9), 2018 and 2020 (10, 40). Chlorophyll *a* data were obtained from the Helgoland Roads time series (63) and have been published for the respective years (40). Metagenome sequencing, assembly and binning (MAGs) are described in (9) (2016) and (10) (2020). Preparation of metaproteome samples (0.2 µm fraction) as well as corresponding LC-MS/MS measurements and data analyses have been described in detail in (9) (2016) and in (40) (2018 and 2020).

Comparative genomics

MAGs from 2016, 2018 and 2020 were dereplicated using dRep v1.14.6 (64) to prevent redundancy, applying a minimum completeness of 70% and contamination lower than 5% at 0.95 ANI (average nucleotide identity). For each representative MAG (555), protein coding sequences for representative MAGs were predicted with Prokka v1.14.6 using default settings

(65). PULs, CAZymes, CBMs, SusC/D-like proteins were predicted as described previously (9), using hmmscan v3.3.2 against dbCAN-HMMdb-V1 and DIAMOND BLASTp v2.1.1.155 (66) against CAZyDB.08062022 provided by dbCAN (67). CBMxx- and CBMyy-containing sequences within representative MAGs and additional draft genomes of previously published 53 North Sea *Bacteroidota* (6) were identified using hmmscan as described above, adding corresponding HMM profiles to the database. Results were further filtered using the hmmscan-parser.sh script from dbCAN with an e-value cutoff of 1E-15 and a minimum coverage of 35%. The distribution of domain organization was visualized with UpSetR (68, 69). The official CAZy classification was applied to semi-manually determine the CBM boundaries, the multimodular compositions, the taxonomic distributions in CAZy and the PUL prevalence and partnerships in PULDB.

Data Availability

The metaproteome datasets for 2018 and 2020, the PDB identifier and SAXS data will be released upon acceptance of the manuscript in a peer-reviewed journal. Metagenome assemblies and MAGs from 2016, 2018 and 2020 phytoplankton blooms are available in the European Nucleotide Archive under the project accessions PRJEB28156 (2016), PRJEB38290 (2018) and PRJEB52999 (2020). Metaproteome data from the 2016 blooms are available in the PRIDE archive (70) through the identifier PXD019294. Phytoplankton data are available on request via Pangaea (https://doi.pangaea.de/10.1594/PANGAEA.864676).

Acknowledgements

This study was supported by the German Research Foundation (DFG) within the research unit FOR 2406 ‘Proteogenomics of Marine Polysaccharide Utilization’ (POMPU) by grants to Hanno Teeling (TE 813/2–3), Dörte Becher (BE 3869/4-3) and Thomas Schweder (SCHW 595/10-3, SCHW 595/11-3). This work also benefited from the support of the Centre National de la Recherche Scientifique (CNRS) and Sorbonne University (Paris). The authors strongly appreciated to have access to the CristalO platform (FR2424, Station Biologique de Roscoff), which is part of the core facility networks Biogenouest and EMBRC-France. We are grateful

for the access to the small-angle X-ray scattering beamline and MX-beamline PROXIMA1 at synchrotron SOLEIL (Saint Aubin, France) and thank the staff for their support on site, especially Aurélien Thureau and Pierre Legrand. We thank the team of the Helgoland sampling campaign, especially Lilly Franzmeyer, and the Biological Station Helgoland (Alfred-Wegener-Institut Helmholtz-Zentrum für Polar- und Meeresforschung, BAH-AWI, Germany), especially Inga Kirstein and Karen Wiltshire. The Helgoland Time Series of the Alfred Wegener Institute is supported by the Helmholtz Association as an LK-II performance category program. We thank Jana Matulla, Jasna Nikolic and Lionel Cladière for support in the lab and Stephanie Markert for helpful comments. MKZ gratefully acknowledges the DFG (SCHW 595/10-3), the PROCOPE Mobility Grant and the ERASMUS Staff Mobility for Training, all of which enabled several research stays in Roscoff.

Author contributions

MC and MKZ directed the study with contribution from EFB and TS. MKZ wrote the first draft of the paper with writing contributions from MC and EFB. All co-authors provided their input on the manuscript and helped with editing. Figures were created by MKZ, MC and DBa. MKZ and MC performed computational sequence analyses of *C. forsetii* proteins. MKZ performed cloning, protein purification as well as experiments on catalytic activity and protein-sugar interactions. NW and RL supported cloning. EFB, MC and MJ supported experiments on protein-sugar interactions. MC and MKZ performed SAXS analyses and data treatment. AJ and MC performed protein crystallography and MC solved the 3D crystal structure. MJ and DJ produced and purified laminarin-derived oligosaccharides. MJ, TE and FT supported protein quality controls. NT classified CBMxx and CBMyy. DBa and NT performed comparative sequence analyses with support of MC and MKZ. DBa analyzed the phytoplankton bloom data with support of FW, HT, ATS and DBe. All co-authors approved the submitted manuscript.

Conflict of Interest

The authors declare no conflict of interest.

References

1. Becker S, Tebben J, Coffinet S, Wiltshire K, Iversen MH, Harder T, et al. Laminarin is a major molecule in the marine carbon cycle. Proc Natl Acad Sci USA. 2020;117(12):6599-607.
2. Read SM, Currie G, Bacic A. Analysis of the structural heterogeneity of laminarin by electrospray-ionisation-mass spectrometry. Carbohydr Res. 1996;281(2):187-201.
3. Gügi B, Le Costaouec T, Burel C, Lerouge P, Helbert W, Bardor M. Diatom-Specific Oligosaccharide and Polysaccharide Structures Help to Unravel Biosynthetic Capabilities in Diatoms. Mar Drugs. 2015;13(9):5993-6018.
4. Vidal-Melgosa S, Sichert A, Francis TB, Bartosik D, Niggemann J, Wichels A, et al. Diatom fucan polysaccharide precipitates carbon during algal blooms. Nat Commun. 2021;12(1):1–13.
5. Koch H, Dürwald A, Schweder T, Noriega-Ortega B, Vidal-Melgosa S, Hehemann JH, et al. Biphasic cellular adaptations and ecological implications of *Alteromonas macleodii* degrading a mixture of algal polysaccharides. ISME J. 2019;13(1):92-103.
6. Kappelmann L, Krüger K, Hehemann JH, Harder J, Markert S, Unfried F, et al. Polysaccharide utilization loci of North Sea *Flavobacteriia* as basis for using SusC/D-protein expression for predicting major phytoplankton glycans. ISME J. 2019;13(1):76-91.
7. Krüger K, Chafee M, Francis TB, del Rio TG, Becher D, Schweder T, et al. In marine *Bacteroidetes* the bulk of glycan degradation during algae blooms is mediated by few clades using a restricted set of genes. ISME J. 2019;13(11):2800-16.
8. Teeling H, Fuchs BM, Becher D, Klockow C, Gardebrecht A, Bennke CM, et al. Substrate-controlled succession of marine bacterioplankton populations induced by a phytoplankton bloom. Science. 2012;336(6081):608-11.
9. Francis TB, Bartosik D, Sura T, Sichert A, Hehemann JH, Markert S, et al. Changing expression patterns of TonB-dependent transporters suggest shifts in polysaccharide

consumption over the course of a spring phytoplankton bloom. ISME J. 2021;15(8):2336-50.

10. Sidhu C, Kirstein IV, Meunier CL, Rick J, Fofonova V, Wiltshire KH, et al. Dissolved storage glycans shaped the community composition of abundant bacterioplankton clades during a North Sea spring phytoplankton bloom. Microbiome. 2023;11(1):77.

11. Unfried F, Becker S, Robb CS, Hehemann JH, Markert S, Heiden SE, et al. Adaptive mechanisms that provide competitive advantages to marine bacteroidetes during microalgal blooms. ISME J. 2018;12:2894–906.

12. Becker S, Scheffel A, Polz MF, Hehemann JH. Accurate quantification of laminarin in marine organic matter with enzymes from marine microbes. Appl Environ Microbiol. 2017;83(9).

13. Labourel A, Jam M, Jeudy A, Hehemann JH, Czjzek M, Michel G. The ß-glucanase *Zg*LamA from *Zobellia galactanivorans* evolved a bent active site adapted for efficient degradation of algal laminarin. J Biol Chem. 2014;289(4):2027-42.

14. Labourel A, Jam M, Legentil L, Sylla B, Hehemann JH, Ferrieres V, et al. Structural and biochemical characterization of the laminarinase *Zg*LamC(GH16) from *Zobellia galactanivorans* suggests preferred recognition of branched laminarin. Acta Crystallogr D. 2015;71:173-84.

15. Pollet RM, Martin LM, Koropatkin NM. TonB-dependent transporters in the Bacteroidetes: Unique domain structures and potential functions. Mol Microbiol. 2021;115(3):490-501.

16. Ratliff AC, Buchanan SK, Celia H. The Ton Motor. Front Microbiol. 2022;13.

17. Glenwright AJ, Pothula KR, Bhamidimarri SP, Chorev DS, Baslé A, Firbank SJ, et al. Structural basis for nutrient acquisition by dominant members of the human gut microbiota. Nature. 2017;541(7637):407-11.

18. Anderson KL, Salyers AA. Biochemical evidence that starch breakdown by *Bacteroides thetaiotaomicron* involves outer membrane starch-binding sites and periplasmic starch-degrading enzymes. J Bacteriol. 1989;171(6):3192-8.

19. Bjursell MK, Martens EC, Gordon JI. Functional genomic and metabolic studies of the adaptations of a prominent adult human gut symbiont, *Bacteroides thetaiotaomicron*, to the suckling period. J Biol Chem. 2006;281(47):36269-79.

20. Tamura K, Foley MH, Gardill BR, Dejean G, Schnizlein M, Bahr CME, et al. Surface glycan-binding proteins are essential for cereal beta-glucan utilization by the human gut symbiont *Bacteroides ovatus*. Cell Mol Life Sci. 2019;76(21):4319-40.

21. Tamura K, Dejean G, Van Petegem F, Brumer H. Distinct protein architectures mediate species-specific beta-glucan binding and metabolism in the human gut microbiota. J Biol Chem. 2021;296:100415.

22. Mystkowska AA, Robb C, Vidal-Melgosa S, Vanni C, Fernandez-Guerra A, Höhne M, et al. Molecular recognition of the beta-glucans laminarin and pustulan by a SusD-like glycan-binding protein of a marine *Bacteroidetes*. FEBS J. 2018;285(23):4465-81.

23. Jam M, Ficko-Blean E, Labourel A, Larocque R, Czjzek M, Michel G. Unraveling the multivalent binding of a marine family 6 carbohydrate-binding module with its native laminarin ligand. FEBS J. 2016;283(10):1863-79.

24. Kumagai Y, Kishimura H, Lang W, Tagami T, Okuyama M, Kimura A. Characterization of an Unknown Region Linked to the Glycoside Hydrolase Family 17 ß-1,3-Glucanase of *Vibrio vulnificus* Reveals a Novel Glucan-Binding Domain. Mar Drugs. 2022;20(4).

25. Deshmukh UB, Oren A. Proposal of *Christiangramia* gen. nov., *Neomelitea* gen. nov. and *Nicoliella* gen. nov. as replacement names for the illegitimate prokaryotic generic names *Gramella* Nedashkovskaya et al. 2005, *Melitea* Urios et al. 2008 and *Nicolia* Oliphant et al. 2022, respectively. Int J Syst Evol Microbiol. 2023;73(4).

26. Eilers H, Pernthaler J, Peplies J, Glöckner FO, Gerdts G, Amann R. Isolation of novel pelagic bacteria from the German bight and their seasonal contributions to surface picoplankton. Appl Environ Microbiol. 2001;67(11):5134-42.

27. Kabisch A, Otto A, König S, Becher D, Albrecht D, Schüler M, et al. Functional characterization of polysaccharide utilization loci in the marine *Bacteroidetes* '*Gramella forsetii*' KT0803. ISME J. 2014;8(7):1492-502.

28. Mirdita M, Schütze K, Moriwaki Y, Heo L, Ovchinnikov S, Steinegger M. ColabFold: making protein folding accessible to all. Nat Methods. 2022;19(6):679-82.

29. Kelley LA, Mezulis S, Yates CM, Wass MN, Sternberg MJE. The Phyre2 web portal for protein modeling, prediction and analysis. Nat Protoc. 2015;10(6):845-58.

30. Holm L. Dali server: structural unification of protein families. Nucleic Acids Res. 2022;50(W1):W210-W5.

31. Pluvinage B, Hehemann JH, Boraston AB. Substrate recognition and hydrolysis by a family 50 *exo-β*-agarase, Aga50D, from the marine bacterium *Saccharophagus degradans*. J Biol Chem. 2013;288(39):28078-88.

32. Drula E, Garron ML, Dogan S, Lombard V, Henrissat B, Terrapon N. The carbohydrate-active enzyme database: functions and literature. Nucleic Acids Res. 2022;50(D1):D571-D7.

33. Emsley P, Lohkamp B, Scott WG, Cowtan K. Features and development of Coot. Acta Crystallogr D Biol Crystallogr. 2010;66(4):486-501.

34. Hudson KL, Bartlett GJ, Diehl RC, Agirre J, Gallagher T, Kiessling LL, et al. Carbohydrate-Aromatic Interactions in Proteins. J Am Chem Soc. 2015;137(48):15152-60.

35. Robert X, Gouet P. Deciphering key features in protein structures with the new ENDscript server. Nucleic Acids Res. 2014;42(W1):W320-W4.

36. Svergun DI, Petoukhov MV, Koch MHJ. Determination of domain structure of proteins from X-ray solution scattering. Biophys J. 2001;80(6):2946-53.

37. Rudenko O, Thureau A, Perez J. Evolutionary refinement of the 3D structure of multi-domain protein complexes from Small Angle X-ray Scattering data. Proceedings of the 2019 Genetic and Evolutionary Computation Conference Companion (Geccco'19 Companion). 2019:401-2.

784 38. Tria G, Mertens HDT, Kachala M, Svergun DI. Advanced ensemble modelling of
785 flexible macromolecules using X-ray solution scattering. IUCrJ. 2015;2,207-17.
786 39. Bernadó P, Mylonas E, Petoukhov MV, Blackledge M, Svergun DI. Structural
787 characterization of flexible proteins using small-angle X-ray scattering. J Am Chem
788 Soc. 2007;129(17):5656-64.
789 40. Schweder T, Beidler I, Steinke N, Schulze T, Sidhu C, Bartosik D, et al. Alpha-
790 glucans from bacterial necromass indicate an intra-population loop within the marine
791 carbon cycle. 2023. PREPRINT (Version 1) available at Research Square
792 [https://doi.org/10.21203/rs.3.rs-3205445/v1]
793 41. Sainz-Polo MA, González B, Menéndez M, Pastor FIJ, Sanz-Aparicio J. Exploring
794 Multimodularity in Plant Cell Wall Deconstruction: STRUCTURAL AND FUNCTIONAL
795 ANALYSIS OF Xyn10C CONTAINING THE CBM22-1-CBM22-2 TANDEM. J Biol
796 Chem. 2015;290(28):17116-30.
797 42. Henshaw JL, Bolam DN, Pires VMR, Czjzek M, Henrissat B, Ferreira LMA, et al. The
798 family 6 carbohydrate binding module CmCBM6-2 contains two ligand-binding sites
799 with distinct specificities. J Biol Chem. 2004;279(20):21552-9.
800 43. Ficko-Blean E, Stuart CP, Suits MD, Cid M, Tessier M, Woods RJ, et al.
801 Carbohydrate recognition by an architecturally complex alpha-*N*-
802 Acetylglucosaminidase from *Clostridium perfringens*. Plos One. 2012;7(3).
803 44. Boraston AB, Bolam DN, Gilbert HJ, Davies GJ. Carbohydrate-binding modules: fine-
804 tuning polysaccharide recognition. Biochem J. 2004;382:769-81.
805 45. Cartmell A, Lowe EC, Baslé A, Firbank SJ, Ndeh DA, Murray H, et al. How members
806 of the human gut microbiota overcome the sulfation problem posed by
807 glycosaminoglycans. Proc Natl Acad Sci USA. 2017;114(27):7037-42.
808 46. Cota J, Alvarez TM, Citadini AP, Santos CR, Neto MD, Oliveira RR, et al. Mode of
809 operation and low-resolution structure of a multi-domain and hyperthermophilic endo-
810 ß-1,3-glucanase from *Thermotoga petrophila*. Biochem Biophys Res Commun.
811 2011;406(4):590-4.

812 47. Tauzin AS, Kwiatkowski KJ, Orlovsky NI, Smith CJ, Creagh AL, Haynes CA, et al.
813 Molecular Dissection of Xyloglucan Recognition in a Prominent Human Gut Symbiont.
814 Mbio. 2016;7(2):e02134-15.
815 48. White JBR, Silale A, Feasey M, Heunis T, Zhu Y, Zheng H, et al. Outer membrane
816 utilisomes mediate glycan uptake in gut Bacteroidetes. Nature. 2023;618(7965):583-
817 9.
818 49. Cameron EA, Kwiatkowski KJ, Lee BH, Hamaker BR, Koropatkin NM, Martens EC.
819 Multifunctional nutrient-binding proteins adapt human symbiotic bacteria for glycan
820 competition in the gut by separately promoting enhanced sensing and catalysis. Mbio.
821 2014;5(5):e01441-14.
822 50. Poli A, Anzelmo G, Nicolaus B. Bacterial Exopolysaccharides from Extreme Marine
823 Habitats: Production, Characterization and Biological Activities. Mar Drugs.
824 2010;8(6):1779-802.
825 51. Hervé C, Rogowski A, Blake AW, Marcus SE, Gilbert HJ, Knox JP. Carbohydrate-
826 binding modules promote the enzymatic deconstruction of intact plant cell walls by
827 targeting and proximity effects. Proc Natl Acad Sci USA. 2010;107(34):15293-8.
828 52. Najmudin S, Guerreiro CI, Carvalho AL, Prates JA, Correia MA, Alves VD, et al.
829 Xyloglucan is recognized by carbohydrate-binding modules that interact with ß-glucan
830 chains. J Biol Chem. 2006;281(13):8815-28.
831 53. Juncker AS, Willenbrock H, Von Heijne G, Brunak S, Nielsen H, Krogh A. Prediction
832 of lipoprotein signal peptides in Gram-negative bacteria. Protein Sci.
833 2003;12(8):1652-62.
834 54. Lieutaud P, Canard B, Longhi S. MeDor: a metaserver for predicting protein disorder.
835 BMC Genomics. 2008;9.
836 55. Groisillier A, Hervé C, Jeudy A, Rebuffet E, Pluchon PF, Chevolot Y, et al. MARINE-
837 EXPRESS: taking advantage of high throughput cloning and expression strategies for
838 the post-genomic analysis of marine organisms. Microb Cell Fact. 2010;9(45).

839 56. Studier FW. Protein production by auto-induction in high-density shaking cultures.
840 Protein Expr Purif. 2005;41(1):207-34.
841 57. Miller GL. Use of Dinitrosalicylic Acid Reagent for Determination of Reducing Sugar.
842 Anal Chem. 1959;31(3):426-8.
843 58. Manalastas-Cantos K, Konarev PV, Hajizadeh NR, Kikhney AG, Petoukhov MV,
844 Molodenskiy DS, et al. ATSAS 3.0: expanded functionality and new tools for small-
845 angle scattering data analysis. J Appl Crystallogr. 2021;54:343-55.
846 59. Kabsch W. XDS. Acta Crystallogr D Biol Crystallogr. 2010;66(Pt 2):125-32.
847 60. Evans PR, Murshudov GN. How good are my data and what is the resolution? Acta
848 Crystallogr D Biol Crystallogr. 2013;69(7):1204-14.
849 61. McCoy AJ, Grosse-Kunstleve RW, Adams PD, Winn MD, Storoni LC, Read RJ.
850 Phaser crystallographic software. J Appl Crystallogr. 2007;40(Pt 4):658-74.
851 62. Murshudov GN, Skubák P, Lebedev AA, Pannu NS, Steiner RA, Nicholls RA, et al.
852 REFMAC5 for the refinement of macromolecular crystal structures. Acta Crystallogr
853 D. 2011;67:355-67.
854 63. Armonies W, Asmus H, Buschbaum C, Lackschewitz D, Reise K, Rick J. Microscopic
855 species make the diversity: a checklist of marine flora and fauna around the Island of
856 Sylt in the North Sea. Helgol Mar Res. 2018;72.
857 64. Olm MR, Brown CT, Brooks B, Banfield JF. dRep: a tool for fast and accurate
858 genomic comparisons that enables improved genome recovery from metagenomes
859 through de-replication. ISME J. 2017;11(12):2864-8.
860 65. Seemann T. Prokka: rapid prokaryotic genome annotation. Bioinformatics.
861 2014;30(14):2068-9.
862 66. Buchfink B, Reuter K, Drost HG. Sensitive protein alignments at tree-of-life scale
863 using DIAMOND. Nat Methods. 2021;18(4):366-8.
864 67. Zheng J, Hu B, Zhang X, Ge Q, Yan Y, Akresi J, et al. dbCAN-seq update: CAZyme
865 gene clusters and substrates in microbiomes. Nucleic Acids Res. 2023;51(D1):D557-
866 D63.

867 68. Lex A, Gehlenborg N, Strobelt H, Vuillemot R, Pfister H. UpSet: Visualization of
868 Intersecting Sets. Ieee T Vis Comput Gr. 2014;20(12):1983-92.
869 69. Conway JR, Lex A, Gehlenborg N. UpSetR: an R package for the visualization of i
870 ntersecting sets and their properties. Bioinformatics. 2017;33(18):2938-40.
871 70. Perez-Riverol Y, Bai J, Bandla C, García-Seisdedos D, Hewapathirana S,
872 Kamatchinathan S, et al. The PRIDE database resources in 2022: a hub for mass
873 spectrometry-based proteomics evidences. Nucleic Acids Res. 2022;50(D1):D543-
874 D52.

875